Experimental and Theoretical Investigation of the Lamellar Structure of a Styrene−Butyl Methacrylate Diblock Copolymer by Fluorescence Resonance Energy Transfer, Small-Angle X-ray Scattering, and Self-Consistent-Field Simulations

John G. Spiro, Jian Yang,† Jian-Xin Zhang,‡ and Mitchell A. Winnik*

Department of Chemistry, University of Toronto, 80 St. George St., Toronto, Ontario, Canada M5S 3H6

Yahya Rharbi

Laboratoire de Rhéologie, BP53-Domaine Universitaire, 38041 Grenoble Cedex 9, France, and Department of Chemistry, University of Toronto, 80 St. George St., Toronto, Ontario, Canada M5S 3H6

Jeffrey D. Vavasour and Mark D. Whitmore

Department of Physics and Astronomy, University of Manitoba, Winnipeg, Manitoba, Canada R3T 2N2

Robert Jérôme

Center for Education and Research on Macromolecules, University of Liège, Sart-Tilman B6, 4000 Liège, Belgium

Received December 5, 2005; Revised Manuscript Received June 19, 2006

ABSTRACT: We have investigated the repeat distance and interface thickness, at 160 °C, of a poly(styrene-*b*-butyl methacrylate) (PS-*b*-PBMA) diblock copolymer of ∼180 000 molecular weight by small-angle X-ray scattering (SAXS) and fluorescence resonance energy transfer (FRET). We have found a lamellar period of 47 nm and an interface thickness of 5 nm. A simple, hyperbolic secant model of the junction distribution appeared to be sufficient to analyze the fluorescence decay data on the junction-labeled polymer containing different acceptor/donor ratios, but simulations based on a numerical self-consistent-field (NSCF) formalism also allowed us to find a range of approximately 0.017−0.018 for the Flory−Huggins interaction parameter (χ_{FH}, defined with reference to the monomeric volume of polystyrene) and a PBMA Kuhn length (b_{PBMA}) of 0.65−0.67 nm. We note that earlier values of χ_{FH} and b_{PBMA} reported in the literature vary considerably. The NSCF computations suggest that even modest levels of conformational asymmetry perturb the block copolymer morphology. A weakness of our theoretical (NSCF) approach is the compressible nature of PS-*b*-PBMA. However, lattice cluster, equation of state (EOS), or other models that allow for compressibility have not yet been developed to the level of sophistication needed to predict block copolymer repeat distances or interface thicknesses. Indeed, as detailed in the Supporting Information, current EOS methods leave much to be desired even in predicting the phase transitions of lower molecular weight PS-*b*-PBMA samples.

Introduction

Melts of diblock copolymers tend to self-assemble into a variety of microphase-separated, ordered structures, such as lamellae, gyroid, cylinders, and spheres.[1] The nature of the ordered phase depends primarily on the ratio of the block volume fractions, f_A and f_B. When the block copolymer is nearly symmetric ($f_A \approx f_B$), the polymer forms a lamellar superstructure. If the product of the Flory−Huggins interaction parameter and the total block copolymer chain length is large ($\chi_{FH}N \gg 10$, with $N = N_A + N_B$, N_A and N_B being the A and B block lengths, respectively), then the A and B blocks are well-segregated and are separated by a narrow interface.[2,3] Lamellar poly(styrene-*b*-isoprene)[4−9] (PS-*b*-PI) and poly(styrene-*b*-2-vinylpyridine)[10−15] are the block copolymers that have been the most extensively studied. The two components of these diblock copolymers are highly immiscible, and therefore the interface between them is narrow.

However, there has also been considerable interest in poly(styrene-*b*-butyl methacrylate) (PS-*b*-PBMA), a rather different material. It exhibits a rich tapestry of microphase-separated morphologies, and these morphologies have considerable influence on its mechanical properties.[16−19] Furthermore, PS-*b*-PBMA is the first block copolymer that was found to show a lower critical ordering transition (LCOT).[20] In contrast to most block copolymers, in addition to the usual order−disorder transition on heating, it can also undergo microphase separation as the temperature is increased.

It is well-known that for blends of immiscible homopolymers the thickness of the interface greatly affects the overall properties. For instance, Feng, Winnik, and Siemiarczuk[21] attributed the significant film stiffness at elevated temperatures in blends of hard and soft latexes to the evolution of interfaces up to 7 nm thick. Similarly, the behavior of microphase-separated block copolymers has major contributions from the mixed interphase between the relatively homogeneous subdomains.[22] The tensile properties of PS-*b*-PBMA have been attributed to the broad interface between microphases.[16]

* To whom correspondence should be addressed. E-mail: mwinnik@chem.utoronto.ca.

† Current address: Department of Polymer Chemistry, Kyoto University, Nishigyo, Kyoto 615-8510, Japan.

‡ Current address: Polymer Source, Inc., 124 Avro Street, Dorval, Quebec, Canada H9P 2X8.

10.1021/ma0526037 CCC: $33.50
Published on Web 09/07/2006

A considerable amount of theoretical work has been done on predicting the morphology, including the interface thickness (δ), of block copolymers. However, many of the best-known theories assume strong segregation, corresponding to high values of the $\chi_{FH}N$ product. Another frequently used approximation is that the copolymers are conformationally symmetric. It is questionable whether such approximations are suitable for PS-*b*-PBMA. In an earlier paper,[23] dealing with the localization of homopolystyrene (hPS) in its blends with PS-*b*-PBMA, we used numerical self-consistent-field (NSCF) computations[24] that dispense with those assumptions, but there was a great deal of uncertainty about the proper values of some input parameters, particularly the χ_{FH} value and the Kuhn length of PBMA. Before proceeding, we will briefly review what was known about the latter quantities prior to the present research.

First, we should point out that the Flory−Huggins χ_{FH} parameter must be defined in terms of a reference volume V_{ref}. The canonical value is the binary interaction energy density $B = \chi_{FH}RT/V_{ref}$,[25] where R is the gas constant and T is the absolute temperature. In the present paper, we will always report χ_{FH} at the annealing temperature of 160 °C of our PS-*b*-PBMA films and with reference to the monomeric molar volume of PS: 105.0 cm^3 (V_{ref}). The latter value we have obtained by interpolation from Quach and Simha's data;[26] in the actual NSCF computations we employed four significant figures for the PS number density: 5.736 nm^{-3}.

Relatively recent (or relatively well accepted) $\chi_{FH(S/BMA)}$ values available from the literature appear to fall into three classes: In 1998, Schubert and co-workers[27] reported $\chi_{FH} = 0.0098$ for 140 °C and $\chi_{FH} = 0.0081$ for 151 °C. The latter results appear to have been computed with reference to the monomeric volume of polystyrene, quoted as 99.378 cm^3/mol in ref 28. Extrapolation to 160 °C and conversion to our V_{ref} leads to $\chi_{FH} = 0.007$ (approximately). The Stamm group's updated formula, published in 1999,[16] gives the temperature-dependent χ_{FH} value as $\chi_{FH} = (0.0243 \pm 0.0004) - (4.56 \pm 0.169)/T$. The latter result is more consistent with the LCOT behavior of PS-*b*-PBMA, with studies employing a variety of experimental techniques,[29] as well as with the year 2000 review[30,31] of specular neutron reflection (SNR) data on symmetric diblock copolymers of (deuterated) PS and PBMA. With our $V_{ref} = 105.0$ cm^3, the latter formula would lead to $\chi_{FH(S/BMA)} = 0.015$ (approximately) at 160 °C. Because of the well-known effect of deuteration on the magnitude of χ_{FH},[32] these may not be the most appropriate values for us to employ in the study of nondeuterated polymer. The Paul group has recently reported a determination of binary interaction energies for nondeuterated PS/PBMA at three annealing temperatures (120, 150, and 180 °C).[33] The temperature dependence is essentially linear; when interpolating to 160 °C and converting to our V_{ref}, we calculate $\chi_{FH(S/BMA)} \approx 0.029$.

One reason—perhaps the main reason—for the scattered values in the previous paragraph (and even more uncertainty is evident from the literature[33]) is the compressible nature of PS-*b*-PBMA. Already Russell and co-workers, who first discovered[20] a diblock copolymer exhibiting LCOT behavior, namely PS-*b*-PBMA, stated that "assuming an incompressible system characterized by a positive segmental interaction parameter, χ" was likely inappropriate here. However, lattice cluster, equation of state (EOS), or other models that allow for compressibility have not been developed to the level of sophistication needed to predict block copolymer repeat distances or interface thicknesses—likely because of the lack of sufficient information on input parameters required. Typically, "compressible" models only lead to phase diagrams, phase transition temperatures, and scattering intensities.[34−36] Indeed, as detailed in the Supporting Information, in their current state of development, EOS methods leave much to be desired even in predicting the phase transitions of lower molecular weight PS-*b*-PBMA samples. Therefore, to interpret the experimental results reported here, we had to make the best of basic Flory−Huggins theory.

The magnitude of the Kuhn length of PBMA is not known with great certainty. For many years, the Helfand and Sapse value[37] of $b_{PBMA} = 0.61$ nm at ambient temperature was generally accepted, but some results in the literature[38] suggest rather different values. The question of thermal expansion is another uncertainty.[38,39] Indeed, in some of their reports[28,40] Schubert and co-workers considered different "scenarios" for statistical segment lengths, leading to different interpretations of their experimental data. Fortunately, our NSCF computations suggest that matching both the fluorescence and small-angle X-ray scattering (SAXS) results on our PS-*b*-PBMA films requires quite precise estimates and hence establishes values of both $\chi_{FH(S/BMA)}$ and b_{PBMA}. Our best fit value of b_{PBMA} is in fact not much larger than the value of 0.61 cited above.

Earlier studies on the interface thickness of lamellar PS-*b*-PBMA have employed primarily transmission electron microscopy (TEM) and specular neutron reflectivity.[27,30] Of these, neutron reflectivity is far more precise. This technique requires deuteration of the PS block, and the raw data contain a contribution from capillary waves[41] that increases the apparent width of the interface. Correcting the data for the capillary wave contribution in SNR studies remains a challenge. Here, we report the results of fluorescence resonance energy transfer (FRET) measurements of lamellar PS-*b*-PBMA interface thickness. The latter technique does not require deuteration, and the range of the energy transfer is so short that waviness of the dividing surface between the different domains does not affect the results.[42,43]

Our FRET experiments involved a pair of diblock copolymers, essentially identical in molecular weight and composition, with donor (D) and acceptor (A) fluorescent dyes attached to the junctions of the respective samples. Because the two block copolymers had the same composition and block length, their mixtures formed the same microphase-separated morphology. We could then carry out a series of fluorescence decay measurements at different D/A ratios and fit mathematical models to the results. Details will be discussed in the Theory and the Results and Discussion sections. We have also conducted precise measurements by SAXS of the lamellar periods of the labeled samples.

The FRET experiments generated donor fluorescence decay curves whose profiles reflect the influence of the local concentration of acceptors in the system. One cannot obtain D and A distributions from direct analysis of these decay profiles. Instead, one has to construct models based upon the theory of block copolymers and block copolymer interfaces to generate simulated data. The optimized fitting parameters are those that best fit the experimental decay profiles as well as the lamellar spacing determined by SAXS. We used two different approaches to simulating FRET data. One was to fit the FRET data by the hyperbolic secant junction distribution function (eq 7 below) first proposed by Helfand and Tagami.[44] This is the approach that we have used successfully in the past with more strongly segregated block copolymer systems. Because of the weaker segregation of PS−PBMA, and its conformational asymmetry, we also fitted the data by junction distributions generated from NSCF simulations, translating them into simulated donor fluorescence decay profiles.

Table 1. Characteristics of Dye-Labeled PS−PBMA Diblock Copolymers

polymer	M_w	M_w/M_n	PS (wt %)
PS−Phe−PBMA	176 000	1.04	50
PS−An−PBMA	184 000	1.03	50

One of the questions that arise in the NSCF approach is whether the FRET and SAXS measurements made at room temperature represent the equilibrium attained at the annealing temperature of 160 °C. Shull and co-workers[45] compared predictions from self-consistent-field theory to experimental (neutron reflectivity) measurements on films quenched from 160 °C to room temperature and estimated that they had to contend with a 5% volume change. They then translated that to a 5% change in the length scales. But since our films—unlike in neutron reflectivity studies—had not been deposited on silicon wafers, or processed in any way to ensure a preferred orientation of the lamellae, the relevant quantity appears to be the linear contraction, less than 2%. That should not affect much the χ_{FN} and b_{PBMA} ranges we are reporting as equilibrium values for 160 °C.

Experimental Section

Instrumentation. SAXS measurements of the lamellar period of our symmetric PS-*b*-PBMA diblock copolymer were carried out on the ID2 (high brilliance beamline) spectrometer at the European Synchrotron Radiation Facility (ESRF), Grenoble, France. A 2-d detector using a pinhole camera was used to record the SAXS patterns. All the measurements were carried out using an incident X-ray wavelength (λ) of 0.995 Å and a sample-to-detector distance of 10 m. The experimental setup was chosen to obtain a 0.2 mm × 0.2 mm size collimated X-ray beam. The standard procedures for data acquisition and data treatment have been described elsewhere.[46] Measurements covered scattering wave vectors (**Q**) from 0.02 to 0.6 nm^{-1}. The combined background due to the extensional cell and the camera was removed from each SAXS pattern. Recorded scattering intensity distributions were integrated over the azimuthal angle and were analyzed as functions of the scattering vector ($\mathbf{Q} = 4\pi(\sin\theta)/\lambda$, where 2θ is the scattering angle). Fluorescence decay profiles were measured using the single photon timing technique,[47] following the procedure described previously.[43,48] Our experiments employed a spark discharge in 0.5 atm of D_2 as the excitation source. Phenanthrene was excited selectively at 300 nm.

Polymer Synthesis and Characterization. Dye-labeled PS-*b*-PBMA samples were prepared by anionic polymerization. In all of the polymer syntheses, styrene was polymerized anionically in tetrahydrofuran and then end-capped with a 1-aryl-1-phenylethylene derivative. The anion formed was used subsequently to initiate BMA polymerization. For the donor-labeled polymer, the aryl group was 9-phenanthryl. For acceptor-labeled polymer, the aryl group was anthracene attached via the 2-position. References 23 and 49 give further detail on our synthetic and characterization procedures for dye-labeled diblock copolymers of styrene with acrylates or methacrylates. Table 1 shows the characteristics of the two dye-labeled PS-*b*-PBMA samples prepared and used in the present study.

Preparation of Polymer Films for FRET and SAXS Measurements. PS−Phe−PBMA and PS−An−PBMA were each dissolved in toluene (spectrograde, Aldrich) to form 5 wt % solutions. These solutions were mixed to give solutions with different weight ratios of the two polymers. A micropipet was used to measure 140 μL of each solution and spread them onto quartz plates (1 cm × 2 cm). These samples were dried very slowly at room temperature in a box equipped with a small release hole in the presence of a reservoir containing additional toluene solvent in order to minimize the drying rate. In this way we obtained smooth, transparent films of essentially identical thicknesses. Seven samples with different molar fractions (f_{An}) of acceptor-labeled polymer were prepared for the energy transfer study, as shown in Table 2. For SAXS measurements, only films of the two neat dye-labeled PS-*b*-PBMAs were prepared, following the procedure mentioned above. After drying, the samples were annealed in a vacuum at 160 °C overnight. SAXS and FRET measurements were performed at room temperature, immediately after the annealing step.

Table 2. Characteristics of Dye-Labeled PS−PBMA Films Prepared for Energy Transfer Measurements

sample no.	1	2	3	4	5	6	7
f_{An}[a,b]	0	0.28	0.40	0.50	0.59	0.70	1
C_{An} (mM)[a,c]	0	1.5	2.1	2.7	3.2	3.7	5.3

[a] Calculated based on the molecular weight and weight ratio of the two components. [b] $f_{An} = m_{An}/(m_{An} + m_{Phe})$, where m is the mole number of Phe or An in a sample. [c] The values are reported to only two significant figures here; more precise numbers were used in actual computations.

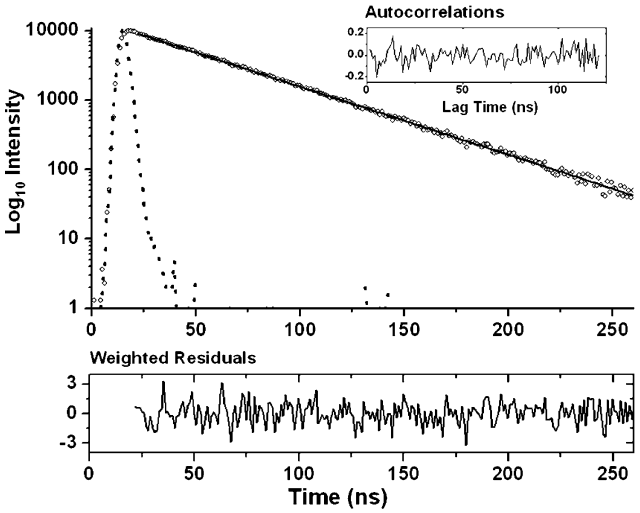

Figure 1. Fluorescence decay curve (scattered points) for neat PS−Phe−PBMA diblock copolymer. The curve was fitted (least-squares algorithm) by a single-exponential term (black line, lifetime 44.0 ns) convoluted with the lamp profile (dotted line, Lamp(t'), obtained by exciting a deaerated solution of *p*-terphenyl in cyclohexane (lifetime: 0.96 ns)), as in the actual experiment. The weighted residuals and autocorrelation function of the residuals are shown as an indication of the goodness of the single-exponential fitting ($\chi^2 = 1.31$).

Energy Transfer Measurements. Fluorescence decays from the donor-labeled diblock copolymer were measured in the absence and in the presence of acceptor labeled diblock copolymer. In each experiment, the phenanthrene (Phe) chromophore was excited at 300 nm, and Phe emission was detected at 350 nm, using a band-pass filter (350 ± 5 nm) to cut off emission from anthracene (An). Background emission from neat PS−An−PBMA was found negligible in the same wavelength range. A total of 10 000 counts were collected in the channel of peak intensity for each sample. The decays were then analyzed using the reconvolution method, which involves comparing the experimental decay curves to the FRET models convoluted with a mimic lamp profile.[50] The mimic lamp profile, used for the convolution analysis,[50] was obtained by exciting a deaerated solution of *p*-terphenyl in cyclohexane (lifetime: 0.96 ns), in the same wavelength range as that for polymer films. Donor fluorescence decay measured from neat Phe-labeled PS-*b*-PBMA was fitted by a single-exponential function. Figure 1 shows the fitting result. We obtained an unquenched donor lifetime of 44.0 ns, with a goodness of fit $\chi^2 = 1.31$.[51]

The Förster radius, R_0, for the Phe−An pair used in this paper was chosen as 2.28 nm. This value was obtained by the spectral overlap method in a PMMA matrix, assuming rapid reorientation of dipoles. A detailed description of the experiments that yielded R_0 can be found in ref 48. The efficiency of energy transfer (Φ_{ET}) is defined by the expression

$$\Phi_{ET} = 1 - \int_0^\infty I_D(t)\,dt / \int_0^\infty I_D^0(t)\,dt \qquad (1)$$

where $I_D(t)$ is the donor fluorescence decay profile and $I_D^0(t)$ is the decay profile in the absence of acceptor. Since the unquenched donor decay is exponential, the denominator in eq 1 can be replaced by the unquenched donor lifetime τ_D. The Φ_{ET} value for each sample listed in Table 2 was calculated by fitting the experimental fluorescence decay using eq 2[52] (here, normalized to unit intensity at zero time) and calculating the area under the curve from eq 3.[53]

$$I_D(t) = \frac{a_1}{a_1 + a_2} \exp\left(-\frac{t}{\tau_D}\right) \exp\left[-\beta\left(\frac{t}{\tau_D}\right)^{0.5}\right] + \frac{a_2}{a_1 + a_2} \exp\left(-\frac{t}{\tau_D}\right) \tag{2}$$

$$\int_0^\infty I_D(t) = \tau_D\left[1 - \left(\frac{a_1\beta}{a_1 + a_2}\right)\frac{\sqrt{\pi}}{2} \exp\left(\frac{\beta^2}{4}\right) \mathrm{erfc}\left(\frac{\beta}{2}\right)\right] \tag{3}$$

In the foregoing equations a_1, a_2, and β are fitting parameters; erfc is the complementary error function. Fifteen years ago,[52] we employed eq 2 to model fluorescence from combinations of "mixed" and "unmixed" domains, but we now find that eq 2 is more useful as a "mathematical French curve" for the analysis of SPC fluorescence decay data.[54]

Numerical Self-Consistent-Field Calculations

NSCF calculations were carried out using the methodology described by Vavasour and Whitmore.[24] The input quantities into these computations also lead to the conformational asymmetry parameter ϵ, defined here as

$$\epsilon = (\rho_{0B} b_B^2)/(\rho_{0A} b_A^2) \tag{4}$$

where ρ_{0P} (P = A or B) are the pure component densities and b_P are the Kuhn lengths for each block. Another, perhaps more important, input parameter is χ_{FH}. As reported in our earlier paper,[23] dealing with blends of PS-*b*-PBMA with homopolystyrene, the degrees of polymerization were 883 for the PS block and 640 for the PBMA block.

Although at first we were not comfortable with the hyperbolic secant approach[42,43,48] to evaluating our FRET data, eventually we found that the NSCF calculations could be replaced to some extent by analysis of the data with reference to a simple Helfand−Tagami distribution function.[44] However, that way we could not extract values of χ_{FH} and b_{PBMA} from our experimental data.

Prediction of the lamellar period (L) by NSCF simulations also led us to consider whether our SAXS measurements were consistent with results reported by Schubert and co-workers.[27,30] We found that, considering the uncertainties of molecular weight determinations (gel permeation chromatography) and of the value α in the scaling law $L \sim N^\alpha$ applicable to our intermediate segregation level,[55] the agreement was satisfactory.

FRET Theory and Simulation Techniques for Lamellar Systems

Many details of FRET theory and its application to lamellar systems were described in our earlier papers;[23,42,43,48] we will be brief here. FRET takes place between the donor (Phe) and acceptor (An) moieties with a rate $w(r)$[56]

$$w(r) = \frac{3}{2}\frac{\kappa^2}{\tau_D}\frac{R_0^6}{r^6} \tag{5}$$

Values of R_0 (2.28 nm) and τ_D (44.0 ns) were determined as described in the Experimental Section. We replaced[48] the orientation factor κ^2 by its preaveraged value: $\langle|\kappa|\rangle^2 = 0.476$, as appropriate for randomly oriented dipoles in rigid media.[57]

Table 3. Physical and Photophysical Parameters That Were Kept Constant in All NSCF and Fluorescence Computations for Films Annealed at 160 °C

PS density (ρ_{PS}): 0.9919 g/cm^3	donor lifetime (τ_D): 44.0 ns
PBMA density (ρ_{PBMA}): 0.9613 g/cm^3	Förster radius (R_0): 2.28 nm
PS Kuhn length (b_{PS}): 0.65 nm	orientation factor ($\langle|\kappa|\rangle^2$): 0.476

In eq 5, r is the distance between a specific donor−acceptor pair; integration over the sample whose fluorescence is monitored leads to the following intensity formula for lamellar systems[58,59]

$$I_D(t) = \exp\{-t/\tau_D\}\int_{-\infty}^{+\infty} C_D(z)\, \psi(z,t)\, \mathrm{d}z \tag{6a}$$

$$\psi(z,t) = \exp\{-g(z,t)\} \tag{6b}$$

$$g(z,t) = 4\pi\int_0^\infty [1 - \exp\{-w(r)t\}]\langle C_A(z,r)\rangle r^2\, \mathrm{d}r \tag{6c}$$

$$\langle C_A(z,r)\rangle = \frac{1}{2r}\int_{z-r}^{z+r} C_A(w)\, \mathrm{d}w \tag{6d}$$

In eq 6, z represents the axis along which concentration profiles vary. Because the intensity is measured in arbitrary units, we have omitted all proportionality constants of eq 6a. The function $\psi(z,t)$ measures the probability that an excited donor, positioned on a plane at z, "survives" for a time t before energy transfer occurs. The exponent function $g(z,t)$ and the mean acceptor concentration $\langle C_A(z,r)\rangle$ are defined to simplify the presentation. Physically, $4\pi r^2 \mathrm{d}r\langle C_A(z,r)\rangle$ may be interpreted as the mean number of acceptors within a shell of radius r and thickness dr surrounding a donor positioned on a plane at z. In eq 6d, the acceptor profile $C_A(w)$ must be in units of number density. To calculate $I_D(t)$, the information needed is the spatial dependence of the donor and acceptor concentration profiles $C_D(z)$ and $C_A(z)$, features determined by the local morphology of the system. Except for simplified calculations, alluded to above and described below, we obtained the donor and acceptor concentrations from the junction distribution probabilities predicted by the NSCF method[24] as functions of the input parameters. Of the latter, values that were considered rather uncertain were the Flory−Huggins χ_{FH} parameter (defined with reference to the monomer volume of PS) and the Kuhn length of PBMA. We varied those. Densities of PS and PBMA (at the annealing temperature) were available from the papers by Quach and Simha[26] and Olabisi and Simha,[60] respectively, and the Kuhn length of PS from the small-angle neutron scattering (SANS) measurements of Boothroyd and co-workers.[61] Table 3 gives the input parameters that were fixed in our NSCF and fluorescence simulations.

Our methods for converting the delta function excitation decays ($I_D(t)$, based on the NSCF junction distributions) to simulated time-correlated single photon counting (SPC) fluorescence decay curves, and how we assess the suitability of the NSCF input parameters by comparing the simulated SPC curves ($I_{sim}(t)$) to experimental fluorescence data, have been published.[23,42] Computation of efficiencies of energy transfer at various acceptor-to-donor ratios, by determining the areas under experimental or simulated SPC curves, was described in the Experimental Section. In such comparisons we also added Poisson noise to the simulated decays.[50]

Considerable simplification of the computations, without much loss of precision, can be accomplished by assuming a hyperbolic secant junction probability distribution[44] which is a direct function of the interface thickness:

$$P_j(z) = \frac{2}{\pi\delta}\,\mathrm{sech}\left(\frac{2z}{\delta}\right) \tag{7}$$

Donor ($C_D(z)$) and acceptor ($C_A(z)$) concentrations are then[50]

$$C_{\mathrm{D}}(z) = \frac{LC_{\mathrm{D}}^0}{2}P_J(z) \tag{8a}$$

and

$$C_{\mathrm{A}}(z) = \frac{LC_{\mathrm{A}}^0}{2}P_J(z) \tag{8b}$$

where C_{D}^0 and C_{A}^0 represent respectively the bulk-averaged concentrations of donor and acceptor groups in the sample. We can now substitute the concentration profiles (8a) and (8b) into eq 6, as described in more detail previously.[42,43,48]

There is one more aspect of FRET theory that we wish to discuss briefly: Perrin model[62] computations.[23] More rigorous calculation of quantum efficiencies of energy transfer (Φ_{ET}) from junction distributions,[43] or comparing experimental time-correlated single photon counting fluorescence decay curves to those obtained by simulations,[42] is time-consuming. We have used such refined techniques mostly to "zero in" on morphological and thermodynamic parameters of interest. But we were also faced with the task of rejecting those input parameters into the NSCF computations[24] that one would otherwise have to consider as alternative conclusions to our studies. In particular, we wanted to examine a fairly broad range of χ_{FH} parameters (because of the controversy surrounding them) and a range of b_{PBMA} values (because the latter had never been measured by suitable techniques). Indeed, we found the Perrin approach very useful and convenient to reject χ_{FH} values in the 0.010−0.016 range (at the annealing temperature: 160 °C).

The Perrin "active sphere" model[62] is an all-or-nothing static quenching model: A quencher within the active quenching sphere quenches the donor fluorescence instantaneously, whereas quenchers outside this sphere have no influence even over long times. Fluorescence intensities computed according to the Perrin model involve reducing the unquenched intensities by a factor $\exp(-\mu)$, where μ is the mean number of quenchers in the active sphere of volume v, with

$$v = \frac{4R_{\mathrm{p}}{}^3\pi}{3} \tag{9}$$

R_{p} being the Perrin radius, and $\exp(-\mu)$ is the Poisson probability that there is no quencher in the sphere.[62] In the formalism we employ[23] we actually compute the number of acceptors, $h(z)$, in a sphere of radius R_{p} centered on a donor positioned at a point z, where the z axis is perpendicular to the planes of the lamellae.

$$h(z) = \pi\int_{z-R_{\mathrm{p}}}^{z+R_{\mathrm{p}}} C_{\mathrm{A}}(z')[R_{\mathrm{p}}{}^2 - (z'-z)^2]\,\mathrm{d}z' \tag{10}$$

In eq 10, $C_{\mathrm{A}}(z)$ is the acceptor concentration, which varies along the z axis, similarly to the donor concentration $C_{\mathrm{D}}(z)$

$$C_{\mathrm{D}}(z) = C_{\mathrm{D}}^0 P(z) \tag{11a}$$

$$C_{\mathrm{A}}(z) = C_{\mathrm{A}}^0 P(z) \tag{11b}$$

C_{D}^0 and C_{A}^0 being the bulk averaged number densities of Phe and An, respectively, and $P(z)$ is the normalized junction probability distribution from the NSCF simulation. The quantum efficiency of energy transfer is then obtained as

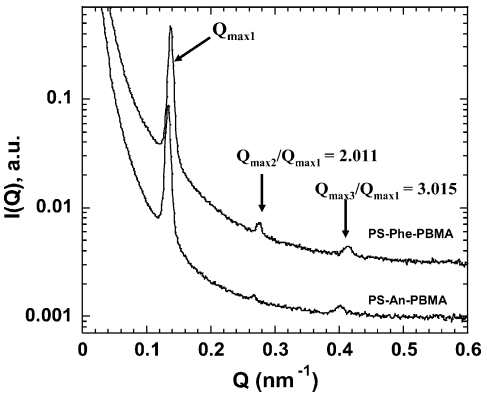

Figure 2. SAXS curves for the dye-labeled diblock copolymers PS−Phe−PBMA and PS−An−PBMA (Table 1), as indicated in the figure. The films were annealed at 160 °C overnight prior to the measurement. For each sample, the peaks marked by the arrows are the ordered scattering peaks. The ratios of the positions (**Q**) of each ordered peak to the first scattering peak position are also shown in the figure for PS−Phe−PBMA.

$$\Phi_{\mathrm{ET}} = 1 - \frac{\int C_{\mathrm{D}}(z)\exp[-h(z)]\,\mathrm{d}z}{\int C_{\mathrm{D}}(z)\,\mathrm{d}z} \tag{12}$$

with the integrations carried out over the element of symmetry: one-half of a lamella. The NSCF results usually give junction probabilities over 101 equidistant points of a half lamella; for fluorescence decay simulations we also need to reflect the junction distributions across the boundaries of the unit cell (cf. eq 10). Fortuitously, the Förster radius, R_0, which can also be used to approximate R_{p}, was similar in our studies to 1/20 of the lamellar period. Thus, we employed $R_{\mathrm{p}} = L/20$ in our Perrin simulations, which very considerably simplified the numerical integrations. Readers will note the similarities between our Perrin model algorithm and the Förster model eqs 6 and 8.

Results and Discussion

The Periodic Structure. The SAXS profiles for films annealed at 160 °C are shown in Figure 2. For both the phenanthrene- and anthracene-labeled block copolymers three maxima are evident in the range of scattering wave vectors (**Q**) investigated. The ratios of the **Q** values relative to the first peak are 1, 2.011, and 3.015 (Figure 2) for PS−Phe−PBMA; they are very similar for PS−An−PBMA. They indicate long-range periodic, lamellar structures with lamellar periods of 46 nm for the phenanthrene-labeled sample and 47 nm for the anthracene-labeled sample. These results imply that the incorporation of small chromophores at the block junctions did not interfere with the lamellar structure, nor did it have a significant effect on the period. Because of the similar structure of these two block copolymers, we imagine that their mixtures, subjected to similar annealing, will also form identical structures with lamellar periods ranging from 46 to 47 nm.

We were unable to measure the lamellar period satisfactorily by SAXS for samples annealed at temperatures lower than 160 °C. We infer that that the annealing conditions used to obtain the data in Figure 2 were necessary for the periodic structures to reach equilibrium, and therefore we used similar conditions to anneal the samples prepared for fluorescence resonance energy transfer studies. Both the SAXS measurements and the

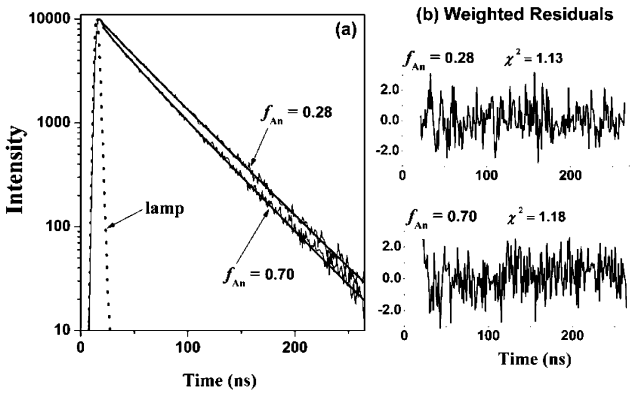

Figure 3. Two experimental fluorescence decays (values of f_{An} are indicated on the graph) from films consisting of PS−Phe−PBMA and PS−An−PBMA copolymer mixtures annealed at 160 °C (Figure 2a). The dotted line is the mimic lamp profile, obtained by exciting a solution of *p*-terphenyl in deaerated cyclohexane (lifetime: 0.96 ns). The solid black lines are the best fits using eqs 6−8 from which the optimized interface thickness was recovered. Weighted residuals and χ^2 of the nonlinear least-squares fitting for the two samples are shown in Figure 2b.

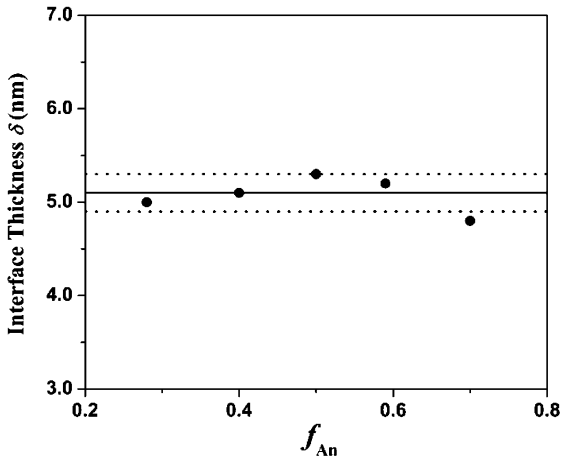

Figure 4. Plot of the optimum values of the interface thickness (filled circles) against the acceptor fraction. The solid line is the averaged value of interface thickness (5.1 nm). The two dotted lines indicate the standard deviation (±0.2 nm).

FRET measurements were carried out at room temperature. We also have to assume that diffusion rates were sufficiently slow after removal of the samples from the oven that no significant rearrangement of the structure took place. This assumption is necessary for us to choose an appropriate temperature for the polymer parameters introduced into the NSCF calculations that describe this system from a theoretical perspective.[45]

Fitting Models of the Block Copolymer Structure to FRET Data. In our experiments, the donor and acceptor dyes are attached to the junctions of the block copolymers, and their distributions, $C_D(z)$ and $C_A(z)$, follow that of the junctions. We measure donor fluorescence decay profiles for various mixtures of donor- and acceptor-labeled polymers and compare the donor decay profiles with simulated decay profiles based upon theories of block copolymer structure. In this analysis, we combine the value of lamellar spacing recovered from SAXS (47 nm) with equations appropriate to calculate the theoretical delta function excitation donor fluorescence decay in the presence of acceptors for different interface thicknesses.

In the section on FRET theory and simulation techniques, we pointed out that these computations are simplified considerably if we assume a hyperbolic secant junction probability distribution[44] which is a direct function of the interface thickness. The basic (Helfand−Tagami) model from which this distribution function was derived makes assumptions of strong segregation and morphological symmetry that do not apply to PS−PBMA, but calculations based on eqs 7 and 8 serve as useful reference points for comparison with the results based on the NSCF computations. We used a procedure similar to that described in ref 50 to fit the calculated decays to the experimental decays measured at the same acceptor fractions. The optimized interface thickness recovered corresponds to the best fits of the experimental decays. We present two fitting results in Figure 3. The optimized values of interface thickness at all acceptor concentrations (Table 2) are shown in Figure 4.

As shown in Figures 3 and 4, determination of the interface thickness based on the Helfand−Tagami formula[44] appears to be very successful, in the sense that we obtained essentially the same optimized interface thickness at different acceptor concentrations. The result was $\delta = 5.1$ nm, with a standard error of only 0.2 nm. Furthermore, there is some theoretical justification for using an hyperbolic secant junction distribution function at our intermediate segregation level: Shull[63] found that hyperbolic profiles were good approximations already for $\chi_{FH}N > 20$. Also, it has been shown[50] that the approach we have described can provide precise values of δ if the period spacing (L) has been measured independently—as in our case. (A slight theoretical weakness is that in ref 63 Shull did not allow for conformational asymmetry, only in later work,[45] dealing with stronger segregation.)

We note that the interface thickness of 5 nm is considerably broader than values that were found for PS-*b*-PI[4] and poly(isoprene-*b*-methyl methacrylate),[43,48] which are more strongly segregated systems. This is consistent with the χ_{FH} values suggested by our NSCF simulations (see below). It is not known whether compressibility affects the interface thickness for PS-*b*-PBMA. Theoretical work by Cho[64] and experimental studies by Pollard et al.[65] confirm earlier research by Russell and co-workers,[20] suggesting that PS-*b*-PBMA phase separation is driven by a positive volume change. In UCOT (upper critical order transition) systems, excess free volume is expected to be present at the interface to screen unfavorable interactions between domains,[66] but in PS-*b*-PBMA this does not appear to be the case.[66,67] Thus, the interface thickness may not be affected. In the Supporting Information we discuss other uncertainties and imprecisions associated with thermodynamic models incorporating the compressibilities of the PS and PBMA blocks. Likely it was because of those difficulties that most reviewers of our paper considered the "incompressible" χ_{FH} values/range that we report significant and of interest to the polymer community.

From a junction distribution computed by the NSCF method[24] for $\chi_{FH} = 0.022/b_{PBMA} = 0.65$ nm, we obtained simulated quantum efficiencies of energy transfer (Φ_{ET}, eq 1) that were somewhat too high for films annealed at 160 °C (Figure 5). When Φ_{ET} is too high in a simulation, that means that we made assumptions that led to too much quenching, i.e., too thin an interface, because the selected value of χ_{FH} was too large (other things being equal). These exploratory calculations also left something to be desired in the sense that the lamellar period from the NSCF computation was too high (~49 nm); nevertheless, they suggested a somewhat lower χ_{FH} value, perhaps 0.02.

It is of interest to compare the "interface thickness" of the $\chi_{FH} = 0.022/b_{PBMA} = 0.65$ nm NSCF profile to the value of 5.1 nm that we found by the hyperbolic secant approach. We considered two definitions of interface thickness here: (i) full

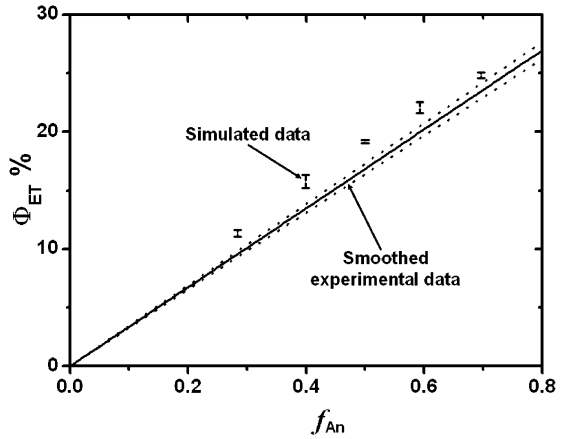

Figure 5. Experimental quantum efficiencies of energy transfer (Φ_{ET}, smoothed by straight line regression through the origin [slope (solid line): 0.337, standard error of the slope (dotted lines): ± 0.009], films annealed at 160 °C) and values obtained from NSCF simulations, plotted against the fraction of acceptor containing block copolymer (f_{An}) in the blends. Input parameters into these NSCF computations were χ_{FH} = 0.022 and b_{PBMA} = 0.65 nm (also see Table 3). SPC curve simulations were carried out in triplicates; the scatter of the results (shown as error bars) is caused by (simulated) Poisson noise.

width at half-maximum (fwhm) of the junction distribution; (ii) the $1/\phi'$ formula: the reciprocal of the derivative $d\phi_{PBMA}/dz$ (where ϕ_{PBMA} is the PBMA volume fraction and z is the distance along the axis perpendicular to the lamellas), calculated at the inflection point $d^2\phi_{PBMA}/dz^2 = 0$. We found 5.4 and 4.4 nm, respectively. It is the second definition that is also employed in the hyperbolic secant approach suggested by Helfand−Tagami theory,[44] again suggesting that χ_{FH} is likely less than 0.022.

Optimizing the Fitting Parameters in the NSCF Model. In this section we compare experimental and simulated donor fluorescence decay curves as well as values of the energy transfer quantum efficiency to identify optimum ranges of the b_{PBMA} and χ_{FH} parameters that describe PS−PBMA at 160 °C in terms of the NSCF model. In connection with the Perrin model computations (see below), we had an extensive set of NSCF junction distributions, obtained for χ_{FH} input values down to 0.01, all of which predicted a lamellar period very close to 47.0 nm (choosing appropriate b_{PBMA} values to achieve this). We selected the $\chi_{FH} = 0.019/b_{PBMA} = 0.636$ nm (L = 46.90 nm) NSCF output for further examination.

Early steps of the SPC curve simulations involve generation of delta function excitation fluorescence decay curves based on the NSCF junction distribution. Upon completing this, we found, rather unexpectedly, that the delta function excitation decays were virtually identical to those that we had obtained for the $\chi_{FH} = 0.022/b_{PBMA} = 0.65$ nm scenario, although the interface thickness increased from 5.4 to 5.9 nm on the fwhm basis and from 4.4 to 4.8 nm on the $1/\phi'$ basis. Clearly, fluorescence decay is dependent on the overall morphology of the dye-labeled block copolymers, governed also by the statistical segment lengths, not only on a somewhat artificial definition of interface thickness.

Since there was hardly any change in the delta function excitation decays (at any of the acceptor concentrations) going from $\chi_{FH} = 0.022/b_{PBMA} = 0.65$ nm to $\chi_{FH} = 0.019/b_{PBMA} = 0.636$ nm, there would be no change in the calculated Φ_{ET}'s; it was unnecessary to pursue that. (The Figure 5 results would apply to the $\chi = 0.019/b_{PBMA} = 0.636$ nm simulations as well.) More information is available by fitting simulated SPC curves to experimental ones.[42] Residual plots[42] that we obtained based on $\chi_{FH} = 0.019/b_{PBMA} = 0.636$ nm NSCF computations (giving a lamellar period of 46.90 nm) suggest that we should reduce χ_{FH}, but only slightly. Indeed, on a $1/\phi'$ basis the latter input parameters lead to an interface thickness of 4.8 nm—not much less than the 5.1 nm we have found by the hyperbolic secant approach.[43,44,50] Essentially, we have confirmed the $\delta = 5.1 \pm 0.2$ nm result, and with the aid of the other NSCF computations plus the Perrin simulations, we can now specify reasonable ranges for $\chi_{FH(S/BMA)}$ and b_{PBMA}.

Table 4. Experimental Quantum Efficiencies of Energy Transfer (Φ_{ET}, %) and Their Estimation by NSCF[24] and Perrin Modeling[23,62] for Various χ_{FH} Parameters and b_{pbma} Values Inputted into the Simulations That Led to Predicted Lamellar Periods between 46.90 and 47.02 nm

	χ_{FH} (b_{PBMA})						
f_{An}	0.010 (0.875)	0.012 (0.798)	0.014 (0.738)	0.016 (0.692)	0.017 (0.673)	0.018 (0.655)	exptl
0.284	6.6	7.5	8.3	9.1	9.5	9.8	10
0.399	9.1	10.3	11.4	12.5	13.0	13.4	13
0.500	11.2	12.7	14.1	15.3	15.9	16.5	16
0.593	13.1	14.8	16.4	17.9	18.5	19.2	19
0.697	15.2	17.2	19.0	20.6	21.4	22.1	25

Table 4 explores, via quantum efficiencies of energy transfer (Φ_{ET}, %) obtained experimentally and by Perrin modeling at different assumed χ_{FH} values, how much lower than 0.019 χ_{FH} is likely to be. As mentioned earlier, the b_{PBMA} input parameters into the NSCF computations were chosen in such a manner that the calculated lamellar periods were very close to the experimental value of 47 nm. f_{An} is the fraction of acceptor-labeled block copolymer in each blend. Reasonable ranges for the NSCF input parameters appear to be 0.017−0.018 for $\chi_{FH(S/BMA)}$ and, correspondingly, about 0.65−0.67 nm (at 160 °C) for b_{PBMA}. The interface thicknesses calculated by the $1/\phi'$ formula are 5.3 nm for χ_{FH} = 0.017 and 5.0 nm for χ_{FH} = 0.018, which agrees with the hyperbolic secant result. However, a word of caution is in order. Likely because of the conformational asymmetries, the $1/\phi'$ definition—although commonly used,[4,44] and although our fluorescence techniques appear to sense this quantity—is *not* equivalent to approximating the interfacial profile by a hyperbolic secant function. This follows from Figure 6, where we show the excellent hyperbolic secant fit we have obtained to the NSCF junction distribution for $\chi_{FH} = 0.017/b_{PBMA} = 0.673$ nm; yet, eq 7 then gives the interface thickness 4.8 nm, whereas from the $1/\phi_{PBMA}'$ definition (ϕ from the NSCF simulation) it is calculated as 5.3 nm (see above). We have to be a little careful about just what we mean by "interface thickness".

To match the lamellar period results in NSCF simulations, we had to vary the b_{PBMA} input values over a fairly broad range.

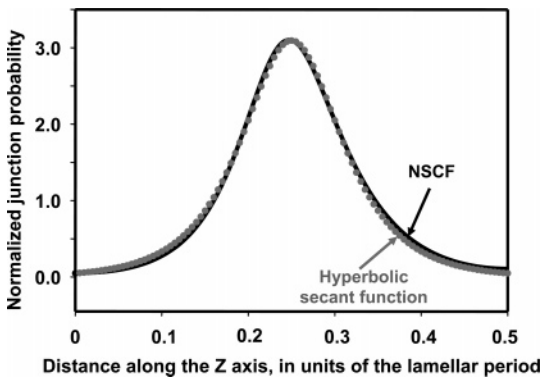

Figure 6. Comparison of the junction distribution (normalized to an average value of unity) from the NSCF simulation with χ_{FH} = 0.017 and b_{PBMA} = 0.673 nm (solid curve, L = 47.02 nm predicted) to its approximation by a hyperbolic secant function (eq 6, circles).

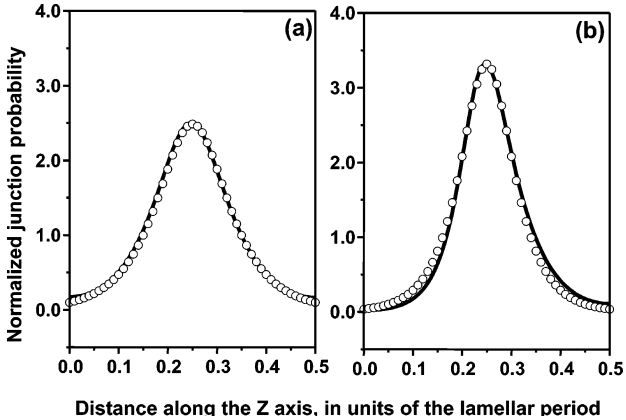

Figure 7. Comparison of hyperbolic secant fits (empty circles) to two different NSCF junction distributions (solid lines). (a) $\chi_{FH} = 0.013$, $\epsilon = 0.9876$ ($b_{PBMA} = 0.767$ nm); (b) $\chi_{FH} = 0.019$, $\epsilon = 0.6047$ ($b_{PBMA} = 0.600$ nm).

Table 5. Quantum Efficiencies of Energy Transfer (Φ_{ET}, %) Estimated by Perrin Modeling[23,62] from the NSCF[24] Junction Distribution for $\chi_{FH} = 0.019$, $\epsilon = 0.6047$ ($b_{PBMA} = 0.600$ nm) and from Its Approximation by the Least-Squares Fit Hyperbolic Secant Function[44] (Eq 7), Both Shown in Figure 7b

	Φ_{ET}, %	
f_{An}	from NSCF	from hyperbolic secant approximation
0.284	8.84	8.83
0.399	12.15	12.13
0.500	14.94	14.92
0.593	17.42	17.39
0.697	20.08	20.05

The NSCF junction and segment density distributions then provided an opportunity to examine the role of conformational asymmetry[24] and other factors. We were particularly interested in exploring how well the hyperbolic secant junction distributions[44] that we frequently employ[42,43,48] agree with the NSCF results. Although the Helfand−Tagami formula is based on assuming strong segregation, we have found that the NSCF junction probability distributions could be fitted well (Figure 7a) with the hyperbolic secant formula even at $\chi_{FH} = 0.013$, $\chi_{FH}N \approx 20$, when the conformational asymmetry was negligible ($b_{PBMA} = 0.767$ nm, $\epsilon = 0.9876$). The quality of the fit strongly deteriorated (Figure 7b) as we reduced b_{PBMA} to 0.60 nm, giving $\epsilon = 0.605$, even though at the latter conditions we were dealing with $\chi_{FH} = 0.019$, $\chi_{FH}N \approx 29$. There were other indications as well that conformational asymmetry perturbs the morphology.

The question now arises: even if an hyperbolic secant approximation to a junction probability distribution leaves something to be desired (Figure 7b—representing a less precise fit than we were aiming for in our earlier studies[23] involving PS-*b*-PBMA), will this have a significant effect e.g. on the quantum efficiencies of energy transfer that we can calculate from it? To answer this question, we conducted further Perrin model[62] computations, similar to those discussed earlier (cf. Table 4). We then compared the results based on the NSCF junction distribution shown in Figure 7b to Perrin model Φ_{ET} values obtainable from the hyperbolic secant approximation, also shown in Figure 7b. The results of the latter computations are given in Table 5. It seems clear that the hyperbolic secant (Helfand−Tagami[44]) approximations are sufficiently precise for fluorescence decay analyses, very likely even for more sophisticated techniques[42] than considering *only* quantum efficiencies of energy transfer.

Conclusions

By fluorescence decay and SAXS measurements, and by interpreting the results in terms of block copolymer and fluorescence resonance energy transfer (FRET) theories, we have found the lamellar period to be 47 nm for PS-*b*-PBMA samples of $M_w = 180\,000$, and the interface thickness to be 5 nm, for films annealed at 160 °C. We note, however, that the concept of interface thickness becomes a little vague for conformationally asymmetric block copolymers. As a "byproduct" of our investigations, we suggest a χ_{FH} value of 0.017−0.018 at 160 °C, with the monomeric volume of PS (105.0 cm^3/mol) as the reference volume; this corresponds to a styrene−BMA interaction energy density[25,33] of 0.14−0.15 cal/cm^3. Our results appear to be in between those reported by the groups of Professors Stamm and Paul, discussed in the Introduction. Matching the measured lamellar period using the foregoing χ_{FH} values gave a PBMA Kuhn length of 0.65−0.67 nm, somewhat higher than the 0.61−0.63 nm range that one would be inclined to accept based on earlier literature data and their usual interpretations,[37,38] but much lower than what other approaches[27,38] would suggest.

To match the measured lamellar period (for films annealed at 160 °C) as well as the fluorescence decay data, we had to consider a range of b_{PBMA} values, leading to a range of conformational asymmetries. We note that conformational asymmetry makes the hyperbolic secant function approximation of junction distributions obtained by self-consistent-field computations less precise. Nevertheless, from the point of view of analyzing florescence decay data, Helfand−Tagami theory appears to be entirely adequate.

A weakness of our theoretical (NSCF) approach is the compressible nature of PS-*b*-PBMA. However, lattice cluster, equation of state, or other models that allow for compressibility have not yet been developed to the level of sophistication needed to predict block copolymer repeat distances or interface thicknesses. Indeed, as detailed in the Supporting Information, if one incorporates the most recent (2004)—and likely most reliable—solubility parameter predictions[68] into the EOS model published by Ruzette and Mayes,[69] one cannot even explain the LCOT behavior discovered by Russell and co-workers[20] for lower molecular weights.

Acknowledgment. The authors thank NSERC Canada for their support of this research. R. Jérôme is grateful to the "Services Fédéraux des Affaires Scientifiques, Techniques et Culturelles" for financial support in the frame of the "Pôles d'attraction Interuniversitaires: 4-11: Chimie Supramoléculaire et Catalyse Supramoléculaire". The authors are also grateful to the European Synchrotron Radiation Facility (ESRF) and for the assistance of Dr. T. Narayanan with the SAXS experiments.

Supporting Information Available: Calculation of the free energy of mixing for our PS-*b*-PBMA samples and implications of the results; possible role of specific interactions for PS-*b*-polymethacrylates; recent experimental and theoretical studies involving PS-*b*-poly(*n*-pentyl methacrylate) copolymers, concluding that the conventional (incompressible) Flory−Huggins approach to data analysis is still quite appropriate. This material is available free of charge via the Internet at http://pubs.acs.org.

References and Notes

(1) Hamley, I. W. *The Physics of Block Copolymers*; Oxford University Press: New York, 1998.
(2) Bates, F. S.; Fredrickson, G. H. *Annu. Rev. Phys. Chem.* **1990**, *41*, 525.
(3) Stamm, M.; Schubert, D. W. *Annu. Rev. Mater. Sci.* **1995**, *25*, 325.

(4) Hashimoto, T.; Shibayama, M.; Kawai, H. *Macromolecules* **1980**, *13*, 1237.
(5) Hasegawa, H.; Hashimoto, T.; Kawai, H.; Lodge, T. P.; Amis, E. J.; Glinka, C. J.; Han, C. C. *Macromolecules* **1985**, *18*, 67.
(6) Hadziioannou, G.; Skoulios, A. *Macromolecules* **1982**, *15*, 258.
(7) Hadziioannou, G.; Picot, C.; Skoulios, A.; Ionescu, M.-L.; Mathis, A.; Duplessix, R.; Gallot, Y.; Lingelser, J.-P. *Macromolecules* **1982**, *15*, 263.
(8) Hasegawa, H.; Hashimoto, T. In *Comprehensive Polymer Science, Suppl. 2*; Aggarwal, S. L., Russo, S., Eds.; Pergamon: London, 1996; pp 497−539.
(9) Mori, K.; Okawara, A.; Hashimoto, T. *J. Chem. Phys.* **1996**, *104*, 7765.
(10) Matsushita, Y.; Mori, K.; Saguchi, R.; Nakao, Y.; Noda, I.; Nagasawa, M. *Macromolecules* **1990**, *23*, 4313.
(11) Matsushita, Y.; Mori, K.; Mogi, Y.; Saguchi, R.; Noda, I.; Nagasawa, M.; Chang, T.; Glinka, C. J.; Han, C. C. *Macromolecules* **1990**, *23*, 4317.
(12) Matsushita, Y.; Mori, K.; Saguchi, R.; Noda, I.; Nagasawa, M.; Chang, T.; Glinka, C. J.; Han, C. C. *Macromolecules* **1990**, *23*, 4387.
(13) Torikai, N.; Matsushita, Y.; Noda, I.; Karim, A.; Satija, S. K.; Han, C. C. *Physica B* **1995**, *213&214*, 694.
(14) Torikai, N.; Noda, I.; Karim, A.; Satija, S. K.; Han, C. C.; Matsushita, Y.; Kawakatsu, T. *Macromolecules* **1997**, *30*, 2907.
(15) Matsushita, Y.; Noda, I.; Torikai, N. *Macromol. Symp.* **1997**, *124*, 121.
(16) Weidisch, R.; Stamm, M.; Schubert, D. W.; Arnold, M.; Budde, H.; Höring, S. *Macromolecules* **1999**, *32*, 3405.
(17) Weidisch, R.; Michler, G. H.; Fischer, H.; Arnold, M.; Hofmann, S.; Stamm, M. *Polymer* **1999**, *40*, 1191.
(18) Weidisch, R.; Michler, G. H.; Arnold, M. *Polymer* **2000**, *41*, 2231.
(19) Weidisch, R.; Stamm, M.; Michler, G, H.; Fischer, H.; Jérôme, R. *Macromolecules* **1999**, *32*, 742.
(20) (a) Russell, T. P.; Karis, T. E.; Gallot, Y.; Mayes, A. M. *Nature (London)* **1994**, *368*, 729. (b) Karis, T. E.; Russell, T. P.; Gallot, Y.; Mayes, A. M. *Macromolecules* **1995**, *28*, 1129.
(21) Feng, J.; Winnik, M. A.; Siemiarczuk, A. *J. Polym. Sci., Part B: Polym. Phys.* **1998**, *36*, 1115.
(22) Spontak, R. J.; Williams, M. C.; Agard, D. A. *Macromolecules* **1988**, *21*, 1377.
(23) Rharbi, Y.; Zhang, J.-X.; Spiro, J. G.; Chen, L.; Winnik, M. A.; Vavasour, J. D.; Whitmore, M. D.; Jérôme, R. *Macromolecules* **2003**, *36*, 1241.
(24) Vavasour, J. D.; Whitmore, M. D. *Macromolecules* **1992**, *25*, 5477.
(25) (a) Paul, D. R. *Pure Appl. Chem.* **1995**, *67*, 977. (b) Zhu, S.; Paul, D. R. *Macromolecules* **2002**, *35*, 2078.
(26) Quach, A.; Simha, R. *J. Appl. Phys.* **1971**, *42*, 4592.
(27) Schubert, D. W.; Weidisch, R.; Stamm, M.; Michler, G. H. *Macromolecules* **1998**, *31*, 3743.
(28) Schubert, D. W.; Abetz, V.; Stamm, M.; Hack, T.; Siol, W. *Macromolecules* **1995**, *28*, 2519.
(29) Fischer, H.; Wedisch, R.; Stamm, M.; Budde, H.; Höring, S. *Colloid Polym. Sci.* **2000**, *278*, 1019.
(30) Schubert, D. W. *Macromol. Symp.* **2000**, *149*, 257.
(31) Matsen, M. W.; Bates, F. S. *Macromolecules* **1996**, *29*, 1091.
(32) Russell, T. P. *Macromolecules* **1993**, *26*, 5819.
(33) Zhu, S.; Paul, D. R. *Polymer* **2003**, *44*, 3963.
(34) Dudowicz, J.; Freed, K. F. *Macromolecules* **1993**, *26*, 213.
(35) Dudowicz, J.; Freed, K. F. *J. Chem. Phys.* **1994**, *100*, 4653.
(36) Hino, T.; Prausnitz, J. M. *Macromolecules* **1998**, *31*, 2636.
(37) Helfand, E.; Sapse, A. M. *J. Chem. Phys.* **1975**, *62*, 1327.
(38) *Polymer Handbook*, 4th ed.; Brandrup, J., Immergut, E. H., Grulke, E. A., Eds.; John Wiley & Sons: New York, 1999; p VII-50.
(39) Lath, D.; Bohdanecky, M. *J. Polym. Sci., Polym. Lett. Ed.* **1977**, *15*, 555.
(40) Schubert, D. W. Ph.D. Thesis, Mainz University; Shaker Verlag: Aachen, 1996.
(41) Sferrazza, M.; Xiao, C.; Jones, R. A. L.; Bucknall, D. G.; Webster, J.; Penfold, J. *Phys. Rev. Lett.* **1997**, *78*, 3693.
(42) Rharbi, Y.; Winnik, M. A. *Macromolecules* **2001**, *34*, 5238.
(43) Yang, J.; Lu, J.; Rharbi, Y.; Cao, L.; Winnik, M. A.; Zhang, Y.; Wiesner, U. B. *Macromolecules* **2003**, *36*, 4485.
(44) Helfand, E.; Tagami, Y. *J. Chem. Phys.* **1972**, *56*, 3592.
(45) Shull, K. R.; Mayes, A. M.; Russell, T. P. *Macromolecules* **1993**, *26*, 3929.
(46) Narayanan, T.; Diat, O.; Bösecke, P. *Nucl. Instrum. Methods Phys. Res. A* **2001**, *467−468*, 1005.
(47) O'Connor, D. V.; Phillips, D. *Time Correlated Single Photon Counting*; Academic Press: London, 1984.
(48) Yang, J.; Roller, R. S.; Winnik, M. A.; Zhang, Y.; Pakula, T. *Macromolecules* **2005**, *38*, 1256.
(49) (a) Hruska, Z.; Vuillemin, B.; Riess, G.; Katz, A.; Winnik, M. A. *Makromol. Chem.* **1992**, *193*, 1987. (b) Ni, S.; Juhué, D.; Moselby, J.; Wang, Y.; Winnik, M. A. *Macromolecules* **1992**, *25*, 496. (c) Ni, S.; Zhang, P.; Wang, Y.; Winnik, M. A. *Macromolecules* **1994**, *27*, 5742.
(50) Yekta, A.; Spiro, J. G.; Winnik, M. A. *J. Phys. Chem. B* **1998**, *102*, 7960.
(51) The χ^2 value is somewhat larger than expected. But the fit is still good, since both the weighted residuals and autocorrelations from the fitting are randomly distributed around zero.
(52) Wang, Y.; Zhao, C. L.; Winnik, M. A. *J. Chem. Phys.* **1991**, *95*, 2143.
(53) *Bateman Manuscript Project, California Institute of Technology. Tables of Integral Transforms*; Erdélyi, A., Ed.; McGraw-Hill: New York, 1954; Vol. I, p 146.
(54) Farinha, J. P. S.; Vorobyova, O.; Winnik, M. A. *Macromolecules* **2000**, *33*, 5863.
(55) Melenkevitz, J.; Muthukumar, M. *Macromolecules* **1991**, *24*, 4199.
(56) Förster, T. *Discuss. Faraday Soc.* **1959**, *27*, 7.
(57) Baumann, J.; Fayer, M. D. *J. Chem. Phys.* **1986**, *85*, 4087.
(58) Yekta, A.; Duhamel, J.; Winnik, M. A. *Chem. Phys. Lett.* **1995**, *235*, 119.
(59) Farinha, J. P. S.; Martinho, J. M. G.; Yekta, A.; Winnik, M. A. *Macromolecules* **1995**, *28*, 6084.
(60) Olabisi, O.; Simha, R. *Macromolecules* **1975**, *8*, 206.
(61) Boothroyd, A. T.; Rennie, A. R.; Wignall, G. D. *J. Chem. Phys.* **1993**, *99*, 9135.
(62) Lakowicz, J. R. *Principles of Fluorescence Spectroscopy*, 2nd ed.; Plenum: New York, 1999; p 245.
(63) Shull, K. R. *Macromolecules* **1992**, *25*, 2122.
(64) Cho, J. *Macromolecules* **2002**, *33*, 2228.
(65) Pollard, M.; Russell, T. P.; Ruzette, A. V.; Mayes, A. M.; Gallot, Y. *Macromolecules* **1998**, *31*, 6493.
(66) Cho, J. *Macromolecules* **2001**, *34*, 6097.
(67) Vogt, B. D. Ph.D. Thesis, University of Massachusetts, Amherst, 2003, p 117.
(68) Utracki, L. A.; Simha, R. *Polym. Int.* **2004**, *53*, 279.
(69) Ruzette, A.-V. G.; Mayes, A. M. *Macromolecules* **2001**, *34*, 1894.

MA0526037